Received: 8 April 2017 | Revised: 22 March 2018 | Accepted: 24 March 2018

DOI: 10.1002/fld.4508

RESEARCH ARTICLE

WILEY

Regularization modelling for large-eddy simulation in wall-bounded turbulence: An explicit filtering-based approach

Tanmoy Chatterjee | Yulia T. Peet

School for Engineering of Matter, Transport and Energy (SEMTE), Arizona State University, Tempe AZ

Correspondence
Tanmoy Chatterjee, ERC 220B, 501 E. Tyler Mall, Arizona - 85281, U.S.A.
Email: tchatte3@asu.edu

Funding information
NSF-CBET, Grant/Award Number: 13358568

Summary

A comprehensive analysis of a filtering-based regularization model for large-eddy simulation has been carried out for fully developed turbulent channel flow, and its potency as a large-eddy simulation candidate has been tested by comparison with eddy-viscosity subgrid-scale models. The exponentially accurate spectral element method, particularly open-source code Nek5000, has been used for such computations. The simulations in the channel flow have been performed at moderately high bulk Reynolds number on the basis of half channel width, 20 000, and compared against the direct numerical simulation database for the mean flow profile, second-order statistics, and their streamwise energy spectra. The results show that the filtering-based regularization model is in reasonably good agreement with the subgrid-scale models, and they also elucidate valuable insights on the filter-based regularization.

KEYWORDS

eddy viscosity, large-eddy simulations, regularization filtering, spectral elements, turbulence

1 | INTRODUCTION

Large-eddy simulation (LES)[1,2] is becoming an increasingly popular technique since the last 3 decades for the study of moderately and high Reynolds number turbulent flows. In LES, the dynamically important large-scale structures of the flow are resolved, whereas small-scale phenomena having a supposedly universal behavior are modeled. The LES methodology represents a viable alternative to direct numerical simulations (DNSs) whose computational cost is prohibitively high at high Reynolds numbers.[3-5] The LES allows many important flow features to be captured without resolving the smaller scales whose effects on the large scales are accounted for by subgrid-scale models.

The computational methodologies that were most frequently realized in the context of LESs until now include strong formulation using finite-difference or mixed finite-difference/pseudospectral methods,[2,6] collocated global spectral methods,[7,8] and finite-difference formulations.[9,10] The application of weak formulation using spectral element methods (SEMs) to LES is relatively less explored, although several works in this domain published since the last decade must be noted.[11-18]

A traditional approach to LES is to generate the differential equations governing the spatio-temporal evolution of large-scale structures, which can be obtained from the Navier-Stokes equations by applying a low-pass filter. The filtering of nonlinear convective product term does not commute with the convection of filtered quantities, which gives rise to an additional term in filtered Navier-Stokes equations called subgrid-scale (SGS) or subfilter-scale term requiring closure. Common approaches to SGS closure include the dissipative eddy-viscosity models, eg, the classic standard or dynamic

Smagorinsky (DS) models[19-21] or the more recent high-pass filtered subgrid model,[22] where the SGS dissipation allows for the dominant forward cascade of energy. More sophisticated approaches based on scale-similarity models,[23,24] mixed models,[25] generalized mixed scale-similarity[26] "inverse models," rational LES models,[27] and approximate deconvolution models[28] have also been proposed in an effort to reconstruct the information of energy spectrum lost by filtering. Traditionally, with these approaches, the low-order finite-difference discretization of the Navier-Stokes equations was used, where the coarse grid acts as an implicit low-pass filter.[1,2,29]

An alternative approach to LES is to work directly with the unfiltered equations resolving the large-scale energy containing eddies and using techniques/models to control the dynamics of the small scales (often based on explicit filtering). In such cases, the SGS term does not explicitly appear in the Navier-Stokes equations exempting additional closure modeling. However, the action of smaller scales must be represented by modifying or *regularizing* the Navier-Stokes equations. Several approaches based on mathematical theories of LES have been developed.[30-32] For the cases of weak solutions of the Navier-Stokes equations (as in SEM), which have not yet testified the uniqueness of solutions in 3D, the regularization proposed in the LES models essentially selects the *physically relevant* solutions.[31,33] Any regularization method designed for LES should guarantee convergence to this physically relevant "dissipative" solution[30] and preserve the spectral accuracy if used with spectral-based schemes such as SEM. The use of SGS models in energy-conserving codes like low-order finite-volume methods provides the only pathway for turbulent kinetic energy to leave the resolved modes and enter the unresolved modes by the correct dissipation characteristics.[34] However, since the regularization models for LES do not satisfy energy conservation, their application in low-order methods have not been explored so far, with the exception of monotone integrated large-eddy simulation approach[35,36] based on conservative flux correction algorithms and specifically designed for use with compressible simulations. The regularization approaches are usually simple to implement, and they have shown good agreement with the benchmark results.[37-39]

It is interesting to note that nearly all of the regularization-type LES approaches were originally designed for the stabilization of higher-frequency (low-energy content) modes arising from the nonlinear convective term.[26,39,40] These approaches include the spectral vanishing viscosity approach by Tadmor,[41] the hyper-viscosity or the p Laplacian ($p > 5/4$) term ∇^p of Lions,[42] and the modification of the Navier-Stokes equations in other works.[30,43-45] In SEM, an effective approach which can be used for stabilization of the Navier-Stokes equations, is by explicit filtering of the solution variables. It must be mentioned that such approaches in LES that use direct explicit filtering of solution variables are quite well-known in compressible LES community[46-48] but are not commonly explored in the incompressible flows. A concise review on regularization models can be found in the monograph by Layton and Rebholz.[49]

The 2 approaches commonly used for SEM filtering are nodal based and modal based.[12,13] In nodal-based methods, filtering projection operators are devised directly from the interpolation polynomials,[50] whereas the modal-based methods design filtering coefficients in the orthogonal polynomial space.[51] The main challenges in the design of filtering for SEM lies in satisfying the boundary conditions for the filtered quantities with spectral accuracy and maintaining an interelement continuity in the filter. The filter-based stabilization approaches have been successfully adopted by the SEM community, see, for example, the work of Levin et al[52] who incorporated the modal filtering procedure[51] to control the growth of nonlinear instabilities in SEM of ocean flows while maintaining spectral accuracy. Fischer and Mullen[50] developed an interpolating polynomial–based nodal filter in SEMs, where the filtering is applied to velocity variable at each time step for stabilization purposes. The interpolation-based filter tested for asymptotic analysis indicated that a mild attenuation of the highest mode was sufficient to stabilize flows in medium-high Reynolds number while retaining interelement continuity and spectral accuracy for the interpolation errors.[53]

Using filter-based regularization (FR) as an LES model is in line with the regularization ideas.[31,33,54] Filter-based regularization models for LES have been used in practical applications that involve rather complex geometries[55-58] and have shown good agreement with experiments or other DNS/LES. However, no detailed comparison for the filtered-based regularization LES models with SGS models is available in the literature. Consequently, a thorough understanding of the performance of the filtered-based regularization model in the SEM formulation and its effect on small-scale motions becomes imperative and is the focus of the current paper.

The present goal involves the validation of the filtering-based regularization LES model in comparison with a well-established scale invariant DS model also developed in the current SEM code. Given the fact that the DS model is computationally more expensive, we particularly aim to explore whether the incorporation of such computationally intensive SGS models provides any advantages in SEM in the framework of LES in wall-bounded flows at moderately high Reynolds numbers. It is important to note that the low-dissipation low-dispersion characteristics of spectral element discretization allow one to decouple the subgrid-scale errors or the filter modeling errors from the numerical errors, which is hard to achieve in low-order methods (see the review by Meneveau and Katz[34] for details).

The results are expected to provide more insights to filtering-based regularization model and the effects of suppressing high-mode information on the large-scale turbulence. For the current study, we use modal-based Boyd filters (with different transfer functions)[12,51,59] for the filter-based model as well as the explicit filtering in DS test case. We also provide some insights on the choice of the filter strength and the number of highest modes to be attenuated in the filtering-based model on the basis of the comparison of channel flow LES statistics with the available DNS data.

2 | NUMERICAL METHOD

The 3D incompressible Navier-Stokes equations, along with boundary conditions, are solved in a weak formulation by means of a weighted residual technique with a Galerkin projection, with inner products in functional spaces using exponentially accurate higher-order SEMs.[53,60-62] The spectral element discretization used in the current study employs collocated methods that involve the same Legendre polynomial spaces for pressure and velocity interpolants, known as $\mathbb{P}_N - \mathbb{P}_N$ formulation, developed as a higher-order splitting technique by Tomboulides et al,[63] with minimum mass conservation errors.

In SEMs,[53,60,62] the decomposition of the computational domain consists of subdividing $\bar{\Omega} = \Omega \cup \partial\Omega$ into E nonoverlapping adjacent rectilinear elements such that $\bar{\Omega} = \cup_{e=1}^{E} \Omega_e$. Each Ω_e is the image of a reference subdomain under a mapping $\mathbf{x}^e(\mathbf{r}) \in \Omega_e \rightarrow \mathbf{r} \in \hat{\Omega}$, with a well-defined inverse $\mathbf{r}^e(\mathbf{x}) \in \hat{\Omega} \rightarrow \mathbf{x} \in \Omega_e$, where the 3D reference subdomain is $\hat{\Omega} = [-1, 1]^3$. Scalar functions within each local element Ω_e are represented as the mth-order tensor product polynomials on a reference subdomain $\hat{\Omega}$. In 3D, velocity and pressure functions in the spectral element method in each element can be expressed as follows:

$$u(r_1, r_2, r_3)|_{\hat{\Omega}} = \sum_{i=0}^{m}\sum_{j=0}^{m}\sum_{k=0}^{m} u^e_{ijk}\pi_{m,i}(r_1)\pi_{m,j}(r_2)\pi_{m,k}(r_3), \quad r_1, r_2, r_3 \in [-1, 1]^3, \tag{1}$$

where, $\pi_{m,i}(r_1)$, $\pi_{m,j}(r_2)$, $\pi_{m,k}(r_3)$ are the Lagrange polynomial–based interpolants of degree m.[53] Because of the invertible mapping between Ω_e and $\hat{\Omega}$, there exists a one-to-one correspondence between the nodal values of $u(x, y, z)|_{\Omega_e}$, $p(x, y, z)|_{\Omega_e}$ and reference subdomain values $u(r_1, r_2, r_3)|_{\hat{\Omega}}$ $p(r_1, r_2, r_3)|_{\hat{\Omega}}$, and the coefficients u^e_{ijk}, p^e_{ijk} are the local nodal values of $u|_{\Omega_e}$, $p|_{\Omega_e}$, respectively, in the nodal-based formulation. The subscripts i, j, k, running from 0 to m within each element for xyz directions, correspond to the roots of the Legendre polynomials, known as the Gauss-Lobato-Legendre (GLL) points. The local to global mapping of data is carried out using a Boolean connectivity matrix that preserves interelement continuity.

Matrix operators in SEM are carried out using computationally efficient tensor/Kronecker products.[53,64] The time discretization of Navier-Stokes solver in the current spectral element code Nek[65] involves third-order backward difference/extrapolation scheme with operator integrator factor splitting–based characteristic time stepping. The code is fully dealiazed using the 3/2 rule,[66,67] the Helmholtz problem for velocity is solved using preconditioned conjugate gradient method, and the pressure solver uses the iterative generalized mean residual solver method in Krylov subspace.

3 | LES MODELS

In this section, we describe 2 LES models used in the current study: DS model[20,21] based on a traditional eddy-viscosity approach to LES involving the low-pass filtered equations and an explicit filtering-based regularization model similar to that in the work of Fischer and Mullen[50] (but using a modal-based approach) used directly in conjunction with the unfiltered equations as a test LES model.

3.1 | Models based on filtered equations

In traditional LES, the "implicitly filtered Navier-Stokes equations" are obtained by invoking a low-pass filter to the Navier-Stokes equations with G as a convolution kernel in a domain Ω. A filtering operation, for example, on a velocity variable, is thus defined as

$$\widetilde{u}_i(\boldsymbol{x}, t) = \int_{\Omega} G(\boldsymbol{x} - \boldsymbol{\xi}) u_i(\boldsymbol{\xi}) \mathrm{d}^3\boldsymbol{\xi},$$

with $\boldsymbol{\xi}, \boldsymbol{x} \in \Omega$, where Ω is the domain of the flow. It is easy to see that this filtering operation accounts for commutativity with linear operators. The commutation error occurs at the nonlinear term of the NS equation, $\tau^{SGS} = \widetilde{u}_i\widetilde{u}_j - \widetilde{u_i u_j}$,

$$\frac{\partial \widetilde{u}_i}{\partial t} + \tilde{u}_j \frac{\partial \widetilde{u}_i}{\partial x_j} = -\frac{1}{\rho}\frac{\partial \widetilde{p^*}}{\partial x_i} + \widetilde{F}_i + \nu \frac{\partial^2 \widetilde{u}_i}{\partial x_j \partial x_j} - \frac{\partial \tau_{ij}^{SGS}}{\partial x_j}, \tag{2}$$

which shows up as the divergence of τ^{SGS} in the momentum equations (see Equation (2). Here, $\widetilde{F}_i$ is the filtered forcing term in the ith direction, and $\widetilde{p^*}$ is defined by

$$\frac{1}{\rho}\widetilde{p^*} = \frac{1}{\rho}\widetilde{p} + \frac{1}{2}\widetilde{u_i^2}. \tag{3}$$

Errors due to the noncommutativity of the filtering and the boundedness of the domain also occur at the boundary of the domain Ω, in the absence of a high enough wall resolution (*boundary commutation errors*), which can be addressed by near-wall modeling but are beyond the scope of the current paper.[1,2] In eddy-viscosity models, one aims at modeling the SGS stress tensor τ_{ij}^{SGS} in the filtered NS equations,[4,20,32,68,69] usually using the gradient of the filtered velocity $\widetilde{u}_i$,[32,69]

$$\tau_{ij}^{\mathrm{SGS}} - \frac{1}{3}\tau_{kk}^{\mathrm{SGS}}\delta_{ij} = -2\nu_t \widetilde{S}_{ij}, \tag{4}$$

where ν_t is the eddy-viscosity and $\widetilde{S}_{ij} = 1/2(\partial\widetilde{u}_i/\partial x_j + \partial\tilde{u}_j/\partial x_i)$ is the filtered strain rate. In Smagorinsky models,[6,19-21,68,70] the interior closure problem of ν_t modeled as $\nu_t = (C_s\Delta)^2|\widetilde{S}|$, where $|\widetilde{S}| = \sqrt{2\widetilde{S}_{ij}\widetilde{S}_{ij}}$, Δ is the characteristic grid filter width, essentially boils down to a physically consistent design of C_s, the Smagorinsky coefficient.

3.1.1 | Dynamic Smagorinsky model

The DS model[20] aims at estimating the Smagorinsky coefficient C_s using a least-squares approach of Lilly[21] from the scale invariance C_s on 2 different filter scales: a grid filter with the width of Δ (usually implicit based on grid discretization) and an explicit coarser test filter with a typical width of $\hat{\Delta} \approx 2\Delta$. In incompressible formulation, divergence-free condition of velocity must be satisfied after the filter is applied. In SEMs, an additional requirement to the filter is that the function interelement continuity must be preserved. In the present spectral element DS model, this can be implemented by using the modal tensor-product approach of Boyd[51] for explicit filtering (which guarantees that function continuity and divergence-free condition of $\widetilde{u}_i$ are satisfied) along the lines of previous literature.[12,13]

With the modal filtering technique, decomposition of the variable u into the modal basis is sought,

$$u(\xi_i) = \sum_{k=0}^{N} \hat{u}_k \phi_k(\xi_i), \tag{5}$$

where $\xi_i, i = 0, \ldots, N$ represents the GLL clustering of the nodes, k represents the number of polynomial modes, and the modal basis $\{\phi\}$, defined as

$$\phi_0 = L_0(\xi), \quad \phi_1 = L_1(\xi) \quad \texttt{and} \quad \phi_k = L_k(\xi) - L_{k-2}(\xi), \quad 2 \le k \le N, \tag{6}$$

forms the hierarchical set of functions constructed from the Legendre polynomials $L_k(\xi)$. Although the Legendre polynomials are normalized, satisfying $L_k(\pm 1) = (-1)^k$, the bubble functions ϕ_k, on the other hand, are designed to preserve homogeneous Dirichlet boundary conditions since $\phi_k(\pm 1) = 0$ for $k \ge 2$. The inhomogeneous Dirichlet boundary conditions are satisfied by the low-order polynomials ϕ_0, ϕ_1. The mapping between the nodal Lagrangian basis and the modal representation defined by Equation (5) can be cast into the matrix form as $\underline{u} = \Phi\underline{\hat{u}}$.

The low-pass filtering is performed in the modal space through a diagonal matrix $\mathbb{T}$ whose diagonal components are $T_0 = T_1 = 1$ (satisfying C_0 interelement continuity) and $T_k = f(k; k_c), 2 \le k \le N$. The function $f(k; k_c)$ is an attenuation function that decreases with increasing k, and k_c is the cut-off value such that $T_k|_{k=k_c} = 1/2$. The filtering process in one dimension is given by

$$\underline{\widetilde{u}} = \mathcal{G} * \underline{u} = \Phi\mathbb{T}\Phi^{-1}\underline{u}. \tag{7}$$

Extrapolation to 3D field can be achieved from 1D filter by a fast tensor product application.[64]

The filtering attenuation function is given by

$$T_k = \frac{1}{1 + (k/k_c)^{\gamma}}, \quad 2 \le k \le N. \tag{8}$$

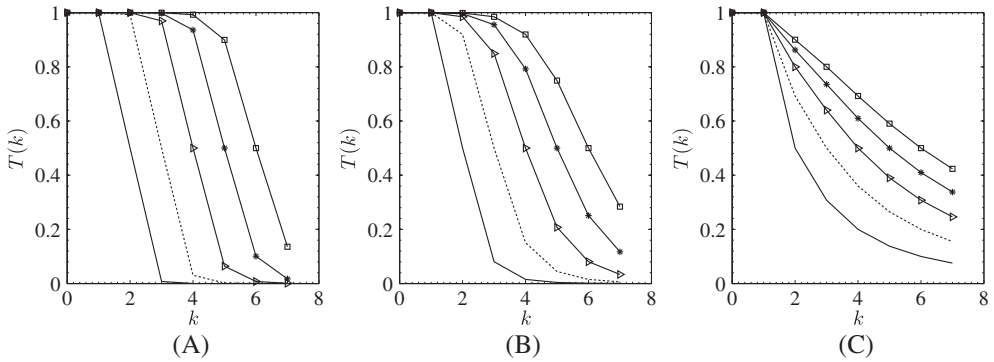

FIGURE 1 Filter transfer function $T(k) = (1 + (k/k_c)^{\gamma})^{-1}$. A, $\gamma = 12$; B, $\gamma = 6$; C, $\gamma = 2$. $-$, $k_c = 2$; $--$, $k_c = 3$; $-.-\triangle k_c = 4$; $-\star$, $k_c = 5$; $-\square$ $k_c = 6 | T(k_c) = \frac{1}{2}$. The total number of modes $k_{\max} = N = 7$ corresponding to Gauss-Lobato-Legendre nodes = 8 (used in our simulation)

The exponent γ in Equation (8) determines the shape of the transfer function, with higher values making the filter function approach a "sharp spectral" filter, with strong attenuation after $k \geq k_c$ and weak attenuation before $k < k_c$, see Figure 1. In our numerical implementation, we utilize $\gamma = 12$ and $k_c = N - 4$ for the DS model, close to sharp filtering ideas of the original DS model.[20] For $N = 7$ employed here, $k_c = N - 4$ corresponds to $k_c = 3$ and is also close to the value of $k_c = (N + 1)/2$ suggested by Blackburn and Schmidt.[12]

With DS model, the subtest stress anisotropy can be written as

$$T_{ij}^{\mathrm{SGS}} - \frac{1}{3} T_{kk}^{\mathrm{SGS}} \delta_{ij} = -2(C_s \hat{\Delta})^2 |\hat{\widetilde{S}}| \hat{\widetilde{S}}_{ij}, \tag{9}$$

$$L_{ij} = T_{ij}^{\mathrm{SGS}} - \hat{\tau}_{ij}^{\mathrm{SGS}} = \hat{\widetilde{u}}_i \hat{\widetilde{u}}_j - \widehat{\widetilde{u}_i \widetilde{u}_j}, \tag{10}$$

where L_{ij} is the resolved part of the stress tensor associated with the scales of motion between the test scale and the grid scale.[20] The closure of the L equation can be given as

$$L_{ij} - \frac{1}{3} L_{kk} \delta_{ij} = 2 C_s^2 M_{ij}, \tag{11}$$

where

$$M_{ij} = \hat{\Delta}^2 |\hat{\widetilde{S}}| \hat{\widetilde{S}}_{ij} - \Delta^2 \widehat{|\widetilde{S}| \widetilde{S}_{ij}}. \tag{12}$$

The least-square estimate obtained from Equation (11), $Q = (L_{ij} - \frac{1}{3} L_{kk} \delta_{ij} - 2 C_s^2 M_{ij})^2$ results in a scale invariance of the Smagorinsky coefficient obtained as

$$C_s^2 = \frac{1}{2} \frac{\langle L_{ij} M_{ij} \rangle}{\langle M_{ij} M_{ij} \rangle}. \tag{13}$$

Evaluating M_{ij}/Δ^2 instead of M_{ij} from Equation (12), we can calculate a local time-dependent value of $C_s \Delta$ instead of C_s at every time step directly from Equation (13) without an explicit definition of Δ in the SGS model. In the current implementation, while solving for turbulent channel flow, which has homogeneous streamwise (x) and spanwise (z) direction, a planar averaging in the $x - z$ direction is performed in the numerator and denominator of $(C_s \Delta)^2$ evaluated from Equation (13) along the lines of Blackburn and Schmidt.[12] Finally, an ad hoc limit of $(C_s \Delta)^2$ is imposed by clipping all the negative values. These 2 additional operations ensure that homogeneity is brute forced in the x, z directions and the values of $(C_s \Delta)^2$ obtained from Equation (13) do not assume negative signs, which otherwise can potentially lead to instability.

3.2 | Regularization model based on unfiltered equations

Regularization models, as discussed above, are based on regularization of unfiltered equations that essentially acts through artificially dissipating the small viscous scales and removing the information of such (unresolved) structures from the flow so that the "dissipative" solutions[30,31,71,72] are naturally favored.

In the current SEM, we consider the modal explicit filtering of primitive variables of the NS equations for regularization. The filtering was originally developed using interpolation techniques in nodal framework for stabilization of unsteady

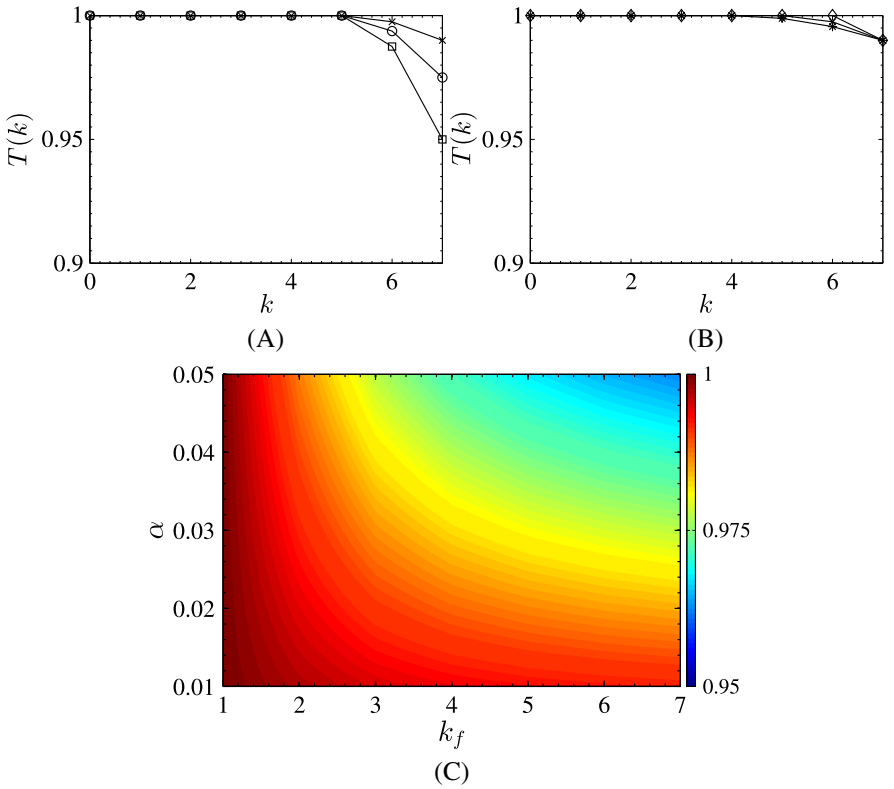

FIGURE 2 Filter transfer function for the regularization model in Equation (14). A, $T(k)$ vs mode k for different $\alpha = 0.01(\times)$, $0.025(\bigcirc), 0.05(\square)$. $k_f = 2$; B, $T(k)$ vs mode k for different $k_f = 1\ (\diamond), 2\ (\times), 3\ (*)$. $\alpha = 0.01$; C, The contour of $T(k)|_{k=N}$ in $\alpha - k_f$ parametric space [Colour figure can be viewed at wileyonlinelibrary.com]

incompressible simulations based on $\mathbb{P}_N - \mathbb{P}_{N-2}$ formulation,[50,53] cutting off only the highest polynomial mode. In the current work, the filtering has been adopted for $\mathbb{P}_N - \mathbb{P}_N$ formulation in LES, with a capability of cutting more than one mode.

The modal filter can be cast along the similar lines as in Equations (5) and (6), with the only difference being in the shape of the filter. In $\mathbb{P}_N - \mathbb{P}_N$ formulation, both the velocity and pressure are filtered at each timestep of the simulation. The filtering attenuation function is quadratic in nature and can be given as

$$T_k = 1 - \alpha\left(\frac{k - N + k_f}{k_f}\right)^2, \quad N - k_f + 1 \leq k \leq N, \tag{14}$$

with $T_0 = T_1 = 1$ and T_k forming the diagonal of the filter-transfer matrix $\mathbb{T}$. In the nodal framework, the 1D filter-transfer function can be defined as $\Phi\mathbb{T}\Phi^{-1}$ (3D filter can be achieved from a 1D filter by tensor product application[64]), with it being a function of parameters α, k_f. The free parameter α determines the amplitude of the filter attenuation, with $\alpha = 1$ corresponding to a sharp cut-off, whereas k_f denotes the number of highest modes that are filtered. In the current regularization model, we use smooth filters with $\alpha = 0.01 - 0.05$ and $k_f = 1 - 3$. The shape of the filter transfer function with mode numbers k at different parameters α, k_f can be found in Figure 2.

4 | NUMERICAL SETUP

To benchmark the performance of the regularization LES model described in the previous section, we perform LES simulations in a turbulent channel flow with 2 different grid resolutions for a moderately high Reynolds number $Re_\delta = 20\,000$, where Reynolds number, $Re_\delta = U_m\delta/\nu$, is based on bulk mean velocity U_m, a half channel width δ, and a kinematic viscosity ν (the corresponding Reynolds number based on skin friction velocity is $Re_\tau = 1000$). The computational domain in the current work is $8\pi\delta \times 2\delta \times 3\pi\delta$ in streamwise, wall-normal, and spanwise directions, respectively, along the lines of moderately high Re simulations in the works of Hoyas et al[73] and Lee and Moser.[74] The different resolutions are generated by the h refinement of SEM while keeping the polynomial order fixed at $N = 7$. The horizontal streamwise (x) and

TABLE 1 Numerical setup for channel flow large-eddy simulation for different grid resolutions

Resolution	$N_x^e \times N_y^e \times N_z^e$	$N_x \times N_y \times N_z$	$N_t(y^+<10)$
1	$60 \times 18 \times 20$	$361 \times 97 \times 121$	2
2	$70 \times 20 \times 30$	$421 \times 121 \times 181$	4
DNS[74]	$--$	$2304 \times 512 \times 2048$	$\sim 10 - 20$

Abbreviation: DNS, direct numerical simulation.

TABLE 2 Grid resolution in wall plus units for $Re_\delta = 20\,000 (Re_\tau = 10\,000)$. y^+ resolution: subscript w is for wall, c is for inviscid core

Resolution	$\Delta x^+_{\min}$	$\Delta x^+_{\max}$	$\Delta z^+_{\min}$	$\Delta z^+_{\max}$	$\Delta y^+_{\min,w}$	$\Delta y^+_{\max,w}$	$\Delta y^+_{\min,c}$	$\Delta y^+_{\max,c}$
1	26.37	87.71	30.23	98.68	1.8	6.0	19.51	63.7
2	23.05	75.18	20.15	65.78	1.64	5.37	17.86	58.31
DNS[74]	10.9	10.9	4.6	4.6	0.019	0.019	4.5	4.5

Abbreviation: DNS, direct numerical simulation.

spanwise (z) directions have been uniformly discretized with the elements, whereas wall normal $y \in (-\delta, \delta)$ direction has been discretized with the clustered elements near the wall (using a hyperbolic sine stretching). For the present LES computations, the number of elements and the number of grid points used in the channel flow LES for all the test cases are shown in Table 1. Here, N_i^e are N_i are, respectively, the number of elements and the number of grid points in the ith direction, where $i = x, y, z$. N_t indicates the number of grid points above the wall that has been used in the region $y^+ < 10$.

Moreover, LESs with 2 different grid resolutions have been performed in the current study, with the grid parameters summarized in Table 1 and resolution in wall units (normalized by $\delta_\nu = \nu/u_\tau$) documented in Table 2. As can be seen from the design of the grids in Table 1, the near-wall resolution is such that the number of grid points in the viscous sublayer N_t is less than 5, which corresponds to *coarsely resolved* LES. This low near-wall resolution has been chosen purposely to better illustrate the effect of filtering in the regularization LES model on the results. With finer resolutions, the effect of filtering would be less conspicuously pronounced. Although DS LESs in SEM have been previously applied in the context of wall-resolved LES[12] with $N_t > 10$; in the current work, we restrict DS model to the same coarse grids as the filter-based models, thus presenting a more stringent test for the spectral element LES simulations.

The LESs (cases 1 and 2) have been run until the statistical stationarity was achieved (until flow-through time $tU_m/L_x = 50$), after which statistics were collected for additional time of $tU_m/L_x = 100$. The time stepping of DS model, compared to the FR model, is $\Delta t_{\text{DS}} \approx \frac{1}{2}\Delta t_{\text{FR}}$ to ensure numerical stability. In addition, the DS model also requires more operations per time step for model-related computations on top of the basic Navier-Stokes solver, resulting in an overall computational cost for the DS model being slightly more than doubled as compared with the FR model (see the appendix for details regarding the algorithmic complexity and computational time of the LES models used).

The boundary conditions for the channel flow are periodic in the streamwise and spanwise directions, and no-slip boundary conditions are incorporated for the top and the bottom walls in the vertical direction.

For the current LES computations, the regularization model and the DS model will be validated with the channel flow DNS results[74] at the corresponding Reynolds number $Re_\tau = 1000$. For the FR technique, we have tested filter weights $\alpha = 0.01 - 0.05$ and 3 different choices for the cutoff wavenumber in the filter function (the number of filtered modes) $k_f = 1, 2, 3$. The complete list of cases run for the current LES computations at 2 different grid resolutions is presented in Table 3. As can be seen from the Table 3, along with the filtering-based model with varying α, k_f, and DS model, we have also performed the simulations with $\alpha = 0$ corresponding to a coarse DNS with no filter, in an effort to decouple the effects of filtering from that of projection (due to a coarse grid) in the LES framework.

5 | RESULTS AND DISCUSSIONS

The mean streamwise velocity and streamwise Reynolds stress are compared for 2 different grid resolutions and benchmarked against the DNS data in Figure 3. As expected, the finer grid element resolution of $70 \times 20 \times 30$ yields a better

TABLE 3 Different cases of numerical simulations run for the Reynolds number $Re_\delta = 20\,000$ channel flow at 2 different grid resolutions. Case I is a coarse, unresolved direct numerical simulation (no model); Dyn. Smag. refers to the dynamic Smagorinsky model

Case	α	k_f
I	0	–
II	0.01	1
III	0.01	2
IV	0.01	3
V	0.025	2
VI	0.05	2
Dyn. Smag.	–	–

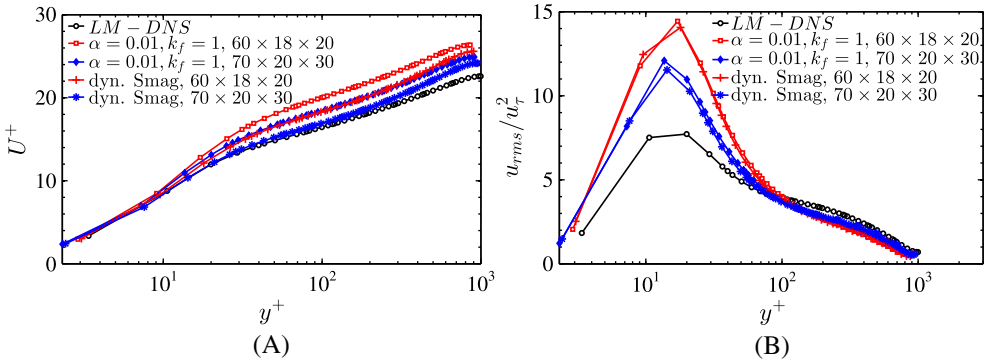

FIGURE 3 Temporally averaged A, mean normalized velocity $U^+ = U/u_\tau$ and; B, streamwise Reynolds stress u_{rms}/u_τ^2 vs y^+ at $Re_\delta = 20\,000$ for resolutions $60 \times 18 \times 20$, $70 \times 20 \times 30$. The presented results are for a filter-based model, $\alpha = 0.01, k_c = 1$, and dynamic Smagorinsky model at 2 different large-eddy simulation resolutions, compared against direct numerical simulation results of Lee and Moser (LM-DNS)[74] [Colour figure can be viewed at wileyonlinelibrary.com]

agreement with the DNS data than its coarser $60 \times 18 \times 20$ counterpart, and only the results of the finer resolution will be presented hereafter.

The mean streamwise velocity, velocity gradient, and statistics of turbulent Reynolds stresses at $Re_\delta = 20\,000$ are shown in Figures 4, 5, and 6. All the plots on the left show the effect of the variation of the filter amplitude α, for fixed $k_c = 2$, whereas the plots on the right show the variation of the filter modes k_c for a fixed value of $\alpha = 0.01$. Both the plots on the left and on the right contain the results from the DS model as well as the validation DNS data.[74] It must be noted that at coarse wall resolutions, the models are unable to capture the correct velocity gradient $\mathrm{d}U/\mathrm{d}y$ (U here is the temporally and horizontally averaged mean velocity), and hence, the friction velocity scale $u_\tau = \sqrt{\tau_w}/\rho$. Normalization of mean streamwise velocity with u_τ annihilates the errors in capturing the viscous sublayer, as seen in the Figures 4A and 4B. The error in u_τ can be explicitly observed in the upper bound of $y^+ = yu_\tau/\nu$ scale, where a lower value of u_τ (underresolved) would be reflected in a lower value of $y^+_{\max}$.

For the mean streamwise velocity as in Figures 4A and 4D, an interesting phenomenon observed is that in spectral element methods, the DS model at moderate wall resolutions behaves strikingly similar to the coarse DNS model ($\alpha = 0$). Furthermore, for the range of α, k_f used in our filtering models, the sensitivity amongst the models for various filter amplitudes α is not conspicuously seen compared with the models with various filter modes k_f. What is however worthwhile to note is the presence of prominent logarithmic trends of the mean streamwise velocity (wider extent of a flat trend of $y^+\mathrm{d}U^+/\mathrm{d}y^+$) in the filtering models similar to DNS, especially in models with $k_c \geq 2$, which are not seen in DS or coarse DNS. Moreover, in the filtering models, the log region is shifted up with higher modes of filtering k_f. In the logarithmic regime, $U^+ \approx \kappa^{-1}\ln(y^+) + B$ for smooth walls, and $U^+ \approx \kappa^{-1}\ln(y^+) + B - \Delta U^+$ for rough-walls with $\Delta U^+ > 0$ increasing with wall-roughness (see the work of Flack et al[75] and the review by Jiménez[76]). The behavior of the filtering models with different k_f is somewhat similar to the rough-wall trends but now only with $\Delta U^+ < 0$, when compared with the DNS profile. For a reference, we note that $\Delta U^+ = -3.32, -3.66, -3.98$ for filtering with $\alpha = 0.01, 0.025, 0.05$, respectively, with fixed $k_f = 2$. For the models with different number of filtered modes k_f, the variation in the shift ΔU^+ is conspicuously

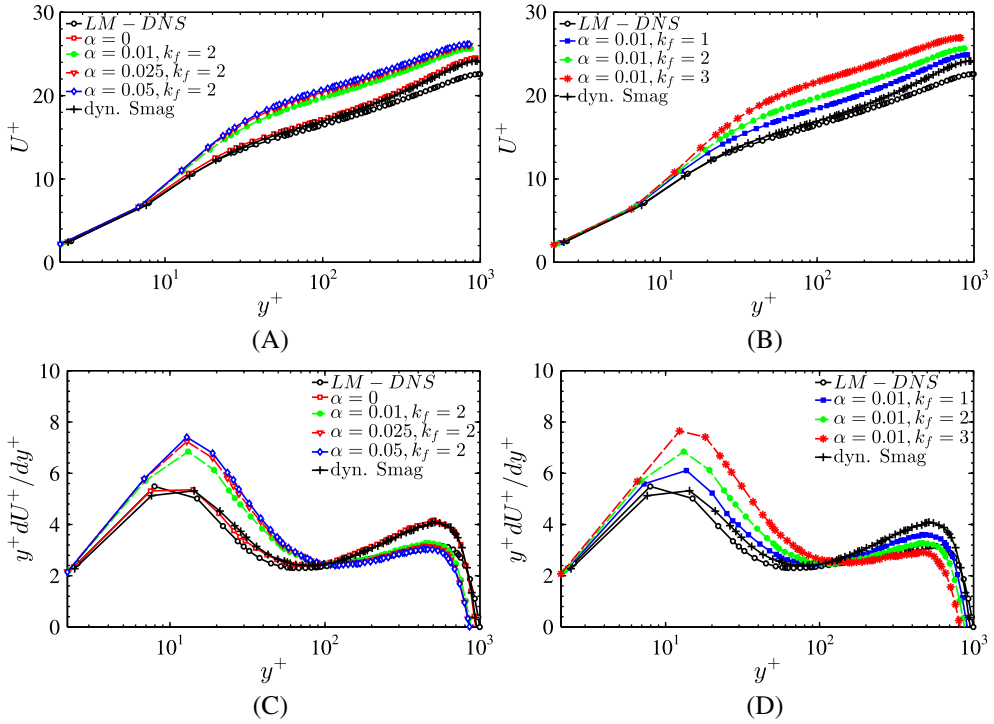

FIGURE 4 Temporally averaged (A), (B) mean normalized velocity $U^+ = U/u_\tau$, and (C), (D) velocity gradient $y^+ \mathrm{d}U^+/\mathrm{d}y^+$ vs y^+ at $Re_\delta = 20\,000$ for filter-based regularization models and dynamic Smagorinsky model compared against direct numerical simulation results of Lee and Moser (LM-DNS).[74] Resolution: $70 \times 20 \times 30$ [Colour figure can be viewed at wileyonlinelibrary.com]

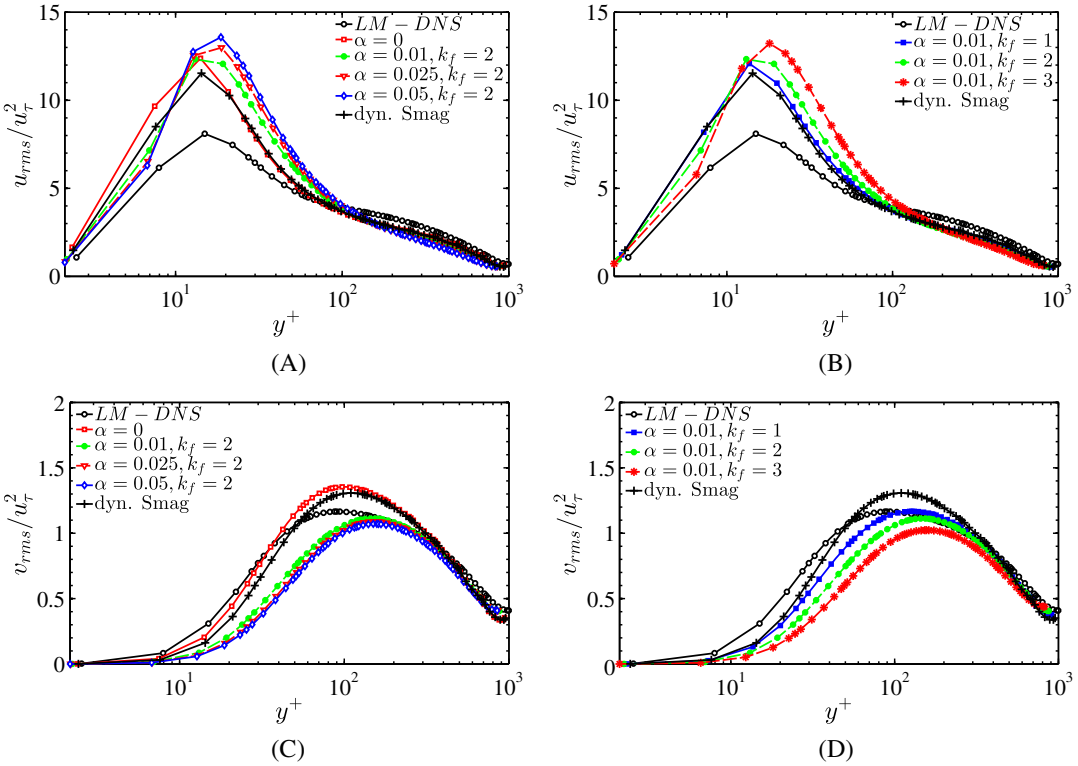

FIGURE 5 Second-order statistics: (A), (B) u_{rms}/u_τ^2 (C), (D) v_{rms}/u_τ^2 vs y^+ at $Re_\delta = 20\,000$ for filter-based regularization models and dynamic Smagorinsky model compared against direct numerical simulation results of Lee and Moser (LM-DNS).[74] Resolution: $70 \times 20 \times 30$ [Colour figure can be viewed at wileyonlinelibrary.com]

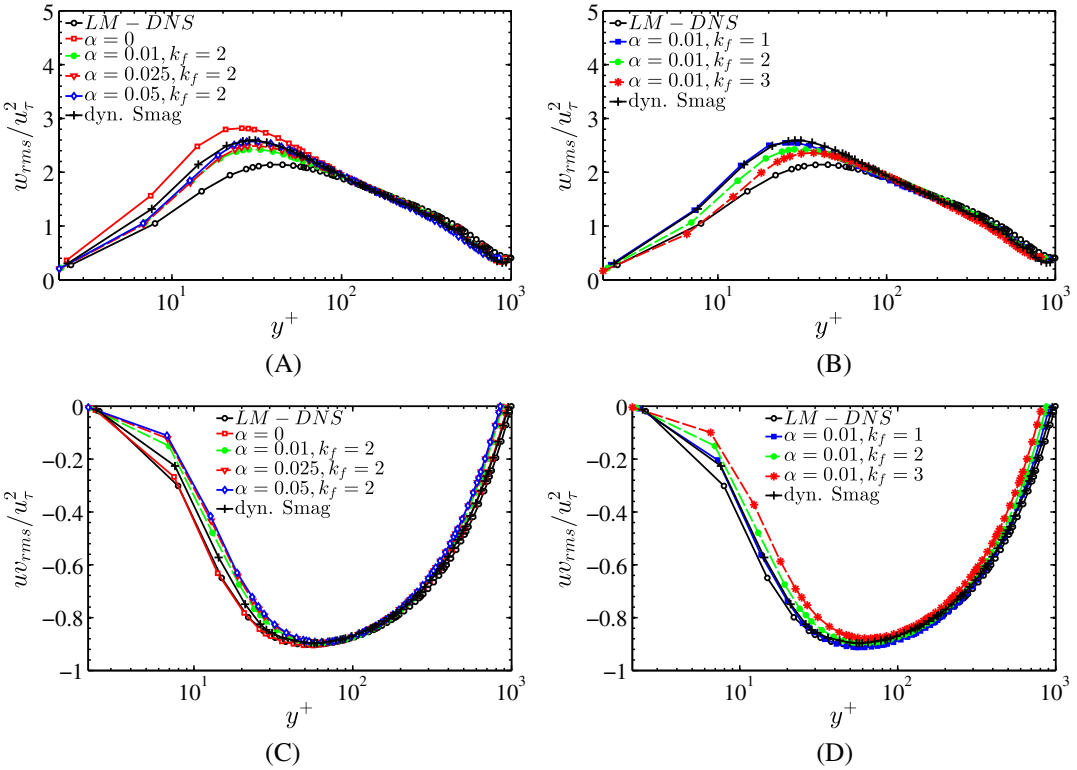

FIGURE 6 Second order statistics: (A), (B) w_{rms}/u_τ^2 (C), (D) uv_{rms}/u_τ^2 vs y^+ at $Re_\delta = 20\,000$ for filter-based regularization models and dynamic Smagorinsky model compared against direct numerical simulation results of Lee and Moser (LM-DNS).[74] Resolution: $70 \times 20 \times 30$ [Colour figure can be viewed at wileyonlinelibrary.com]

stronger, with $\Delta U^+ = -2.05, -3.32, -5.01$, for $k_f = 1, 2, 3$, respectively, with fixed $\alpha = 0.01$. It is worth noting that the mean-velocity statistics in Figure 3A at different resolutions also display a similar phenomenon indicative of the fact that the coarsening of grids behaves similarly to an "explicit filtering." In this sense, it can be speculated that explicit filtering in the current LES models acts as a "negative roughness" by removing small-scale fluctuations from the near-wall region, the point which will be further illustrated by looking at streamwise energy spectra.

The similarity in the behavior of the coarse DNS and DS models is further noticed in the plots of the second-order turbulent statistics normalized with u_τ^2 (Figures 5 and 6), although some discrepancies can be observed in streamwise and, especially, spanwise stresses. In both these fluctuating components, the DS model provides better agreement with the resolved DNS[74] compared with the coarse DNS, which indicates the fact that, although their behavior is generally similar, the presence of the SGS model expectedly manifests the benefits over its absence. The behavior of the filter-based models is generally different from that of the coarse DNS and DS. In all the stresses, filter-based models tend to provide a better agreement with the DNS in the upper log layer and the outer layer while consistently showing worse behavior in the near-wall region. It is interesting to note that all the models do a reasonable job in capturing the trends of the Reynolds shear stress uv_{rms} as seen in Figure 6C, indicating that the Reynolds shear stress are least sensitive to the effects of underresolution and SGS modeling. From our results so far, we can hypothesize that, while filter-based models seem to show the *overdissipative* trends, by providing excessive filtering in the near-wall layer and affecting the near-wall statistics more severely, the coarse DNS and DS models show the *underdissipative* trends, especially in the log layer and outer layer, where insufficient amount of dissipation results in an incorrect energy transfer from the larger to smaller eddies and detrimentally effects the log layer and outer layer statistics. These points will be further corroborated in the analysis of the streamwise energy spectra in the next section.

5.1 | 1D spectra: Re_δ=20 000

At high *Re* flows, high-fidelity experiments,[77-79] as well as emerging high fidelity LES/DNS simulations,[74,80] presented a strong evidence of the universal forms of streamwise energy spectra (eg, k_x^{-1} and $k_x^{-5/3}$ laws, k_x is the streamwise wave

number). The work of Nickels et al[78] has further suggested that only at very high Reynolds number, $Re_\tau \gtrsim 5000$, can a decade long extent of k_x^{-1} law can be expected. For moderately high Reynolds number, $Re_\delta = 20\,000$ ($Re_\tau \sim 1000$), the extent of the inverse law should be supposedly very small. The LES models with $k_f \geq 2$, as well as with $\alpha \sim 0.05$, manifest that a half-decade long region of k_x^{-1} law of one dimensional normalized streamwise energy spectra $E_{uu}(k_x)/(u_\tau^2 y)$ at $y^+ < 50$, which is supposedly an artefact of excessive filtering. While commenting on the k_x^{-1} law is debatable, what is still interesting to note is the presence of $-5/3$ Kolmogorov law[4,69,81] of the energy cascade in the outer layer, which can be observed only in the filtering models. The spectra of coarse DNS, as well as the Smagorinsky model, is quite similarly marked by the complete absence of the $-5/3$ law of the inertial scales even at regions further from the wall $y^+ \sim O(10^2{-}10^3)$. A closer look at Figure 7 also shows that excess filtering ($\alpha = 0.05, k = 2$; $\alpha = 0.01, k = 3$) affects the high wavenumber (smaller length scales) energy content most severely in the near-wall/log-layer region, while it preserves the correct physical trends in the outer layer signal. This is also evidenced by the qualitative picture of the spatial structure in log layer $y^+ \sim 20$ in Figure 8, where smoother streaky structures and reduced small-scale motions are observed with the filter-based model $\alpha = 0.01, k = 3$ (excessive filtering) than with the other models. This leaves a room for hypothesizing the fact that *excessive filtering* might actually be damping scales more severely in the near-wall region in contrast to the DS model, where the mixing length scales supposedly become smaller near the wall promoting less diffusion.[6] However, in the outer layer region, the dissipation of the filter-based models acts positively by removing energy from larger scales of motion and providing a path for the energy transfer to the smaller scales, resulting in improved scaling law predictions

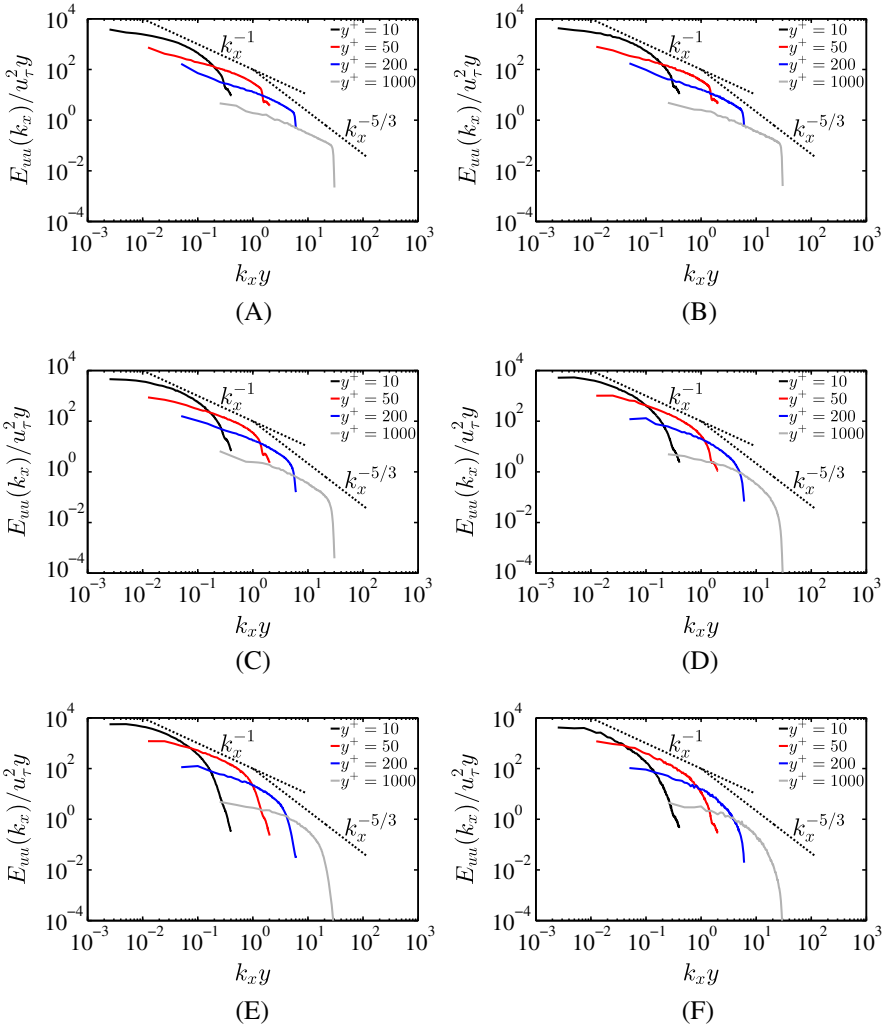

FIGURE 7 Variation of 1-dimensional normalized streamwise energy spectra $E_{uu}(k_x)/(u_\tau^2 y)$ over normalized wavenumber $k_x y$ for different large-eddy simulation models. A, Coarse direct numerical simulation (no model, $\alpha = 0$); B, Dynamic Smagorinsky; C, $\alpha = 0.01, k_f = 1$; D, $\alpha = 0.01, k_f = 2$; E, $\alpha = 0.05, k_f = 2$; F, $\alpha = 0.01, k_f = 3$ [Colour figure can be viewed at wileyonlinelibrary.com]

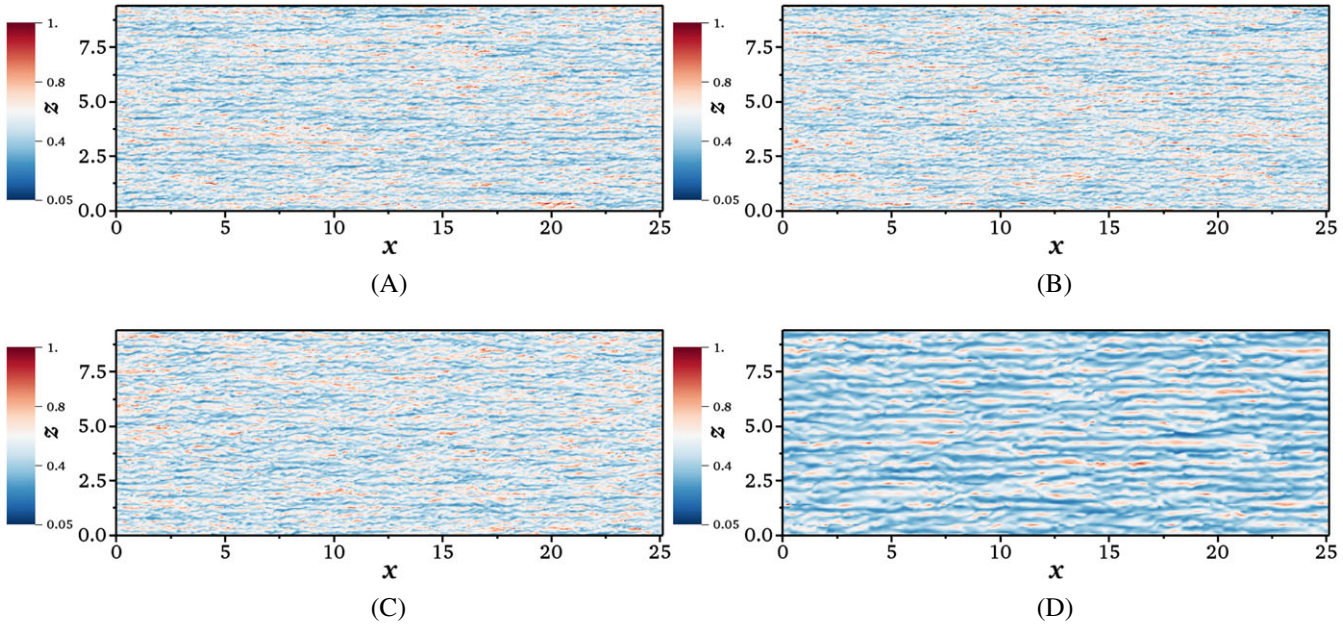

FIGURE 8 Near wall velocity structures at $y^+ = 20$ at Reynolds number $Re_\delta = 20\,000$. A, Coarse DNS; B, Dynamic Smagorinsky; C, Filter model, $\alpha = 0.01, k_f = 1$; D, Filter model, $\alpha = 0.01, k_f = 3$ [Colour figure can be viewed at wileyonlinelibrary.com]

and log-layer behavior with the filter-based models. However, these findings need to be further corroborated by additional studies before a justification is presented.

6 | CONCLUSION AND FUTURE WORK

In the current paper, a comparison of the filtering-based regularization model with the DS model and with the unfiltered coarse DNS has been demonstrated using moderate wall resolutions in SEM. The coarse unfiltered DNS was found to behave similar to DS LES but distinctly different from the filter-based models. The main differences between the 2 groups of models can be summarized in the following facts: (i) the near-wall behavior of the turbulent stresses and the shift in the mean velocity profile were better predicted by DS and the coarse DNS models, whereas (ii) the outer layer statistics, the log-law of the wall, and the Kolmogorov $-5/3$ cascade of the inertial scales were better predicted by the filter-based models. It was therefore concluded that, while the filter-based models seem to provide excessive dissipation (filtering) in the inner layer, the DS and coarse DNS models provide insufficient dissipation (underdissipation) in the outer layer. This leaves room for the surmise that controlling the strength of the filter in the filter-based model might provide a reasonable compromise between the 2 aforementioned effects. In our studies, the filters with $\alpha = 0.01$ and $k_f = 1$ and 2 seemed to yield such a compromise and, overall, represented a competitive counterpart to the DS model. Further potential extension of the current work might lie in designing variable strength filters for LES that reduce the filter strength and/or the number of filtered modes with the distance from the wall, in line with the algebraic damping ideas in eddy-viscosity models. For example, in Smagorinsky-based closures employed in wall-bounded turbulence, where $\nu_t = (C_s\Delta)^2|\widetilde{S}|$ is used as an eddy-viscosity, both dynamic estimations[12] of C_s and wall-damped static models[82] essentially rely on C_s being a function of z (wall-normal coordinate) such as the "filter scale" $C_s\Delta$ decays as we approach the wall. Analogous to wall damping, a z dependence of the parameters α, k_f of the filter-based model can be introduced, which would ensure a gradually less amount of filtering towards the wall. The variable strength filter-based LES can be invoked at a negligible additional cost.

Finally, it is worth noting that, while coarse DNS and DS generally showed similar underdissipative trends, DS consistently produced better results, especially in streamwise and spanwise turbulent stresses, since some amount of useful dissipation is added by the DS model as opposed to no dissipation in the coarse DNS. It is possible that with minimally dissipative high-order methods, higher coefficients are required with eddy-viscosity–type models to provide enough dissipation, whereas the dynamic procedure was not able to provide a sufficiently high coefficient in the outer layer in this context. This hypothesis however needs to be further tested.

ACKNOWLEDGEMENTS

The authors T. Chatterjee and Y. Peet would like to gratefully acknowledge the support of NSF-CBET 13358568 grant for the present work.

ORCID


Tanmoy Chatterjee http://orcid.org/0000-0003-4992-5453

REFERENCES

1. Deardorff JW. Numerical study of three-dimensional turbulent channel flow at large Reynolds number. *J Fluid Mech*. 1970;41(2):453-480.
2. Schumann U. Subgrid scale model for finite difference simulations of turbulent flows in plane channels and annuli. *J Comp Phys*. 1975;18(4):376-404.
3. Reynolds WC. The potential and limitations of direct and large eddy simulations. In: Lumlery JL, ed. *Whither Turbulence? Turbulence at the Crossroads*. Berlin, Germany: Springer-Verlag; 1990:313-343.
4. Pope SB. *Turbulent Flows*. New York, NY: Cambridge University Press; 2000.
5. Piomelli U, Balaras E. Wall-layer models for large eddy simulations. *Annu Rev Fluid Mech*. 2002;34(6):349-374.
6. Porté-Agel F, Meneveau C, Parlange MB. A scale-dependant dynamics model for large eddy simulation: application to a neutral atmospheric boundary layer. *J Fluid Mech*. 2000;415:261-284.
7. Grinstein F, Margolin L, Rider W. *Implicit Large Eddy Simulation: Computing Turbulent Fluid Dynamics*. New York, NY: Cambridge University Press; 2007.
8. Lodato G, Castonguay P, Jameson A. Structural LES modeling with high-order spectral difference schemes. Paper presented at: 42nd AIAA Fluid Dynamics Conference and Exhibit; 2011; New Orleans, LA.
9. Balaras E, Benocci C, Piomelli U. Two-layer approximate boundary conditions for large-eddy simulations. *AIAA J*. 1996;34(6):1111-1119.
10. Piomelli U. High Reynolds number calculation using the dynamic subgrid-scale stress model. *Phys Fluids A*. 1993;5(6):14-84.
11. Karamanos GS, Sherwin SJ, Morrison JF. Large eddy simulation using unstructured spectral/HP elements. In: Knight D, Sakell L, eds. *Recent Advances in DNS and LES*. Dordrecht, Netherlands: Springer; 1999:245-256.
12. Blackburn HM, Schmidt S. Spectral element filtering techniques for large eddy simulation with dynamic estimation. *J Comput Phys*. 2003;186(2):610-629.
13. Bouffanais R, Deville MO, Leriche E. Large-eddy simulation of the flow in a lid-driven cubical cavity. *Phys Fluids*. 2007;19(5):1-20.
14. Wasberg CE, Gjesdal T, Reif BAP, Andreassen O. Variational multiscale turbulence modelling in a high order spectral element method. *J Comput Phys*. 2009;228(19):7333-7356.
15. Chatterjee T, Peet Y. Large eddy simulation of a 3×3 wind turbine array using actuator line model with spectral elements. Paper presented at: 34th Wind Energy Symposium; 2016; San Diego, CA. https://doi.org/10.2514/6.2016-1988
16. Chatterjee T, Peet Y. Spectra and large eddy structures in the double log-layer in a high *Re* wind turbine array boundary layer. Paper presented at: ASME Turbo Expo 2016: Turbomachinery Technical Conference and Exposition; 2016; Seoul, South Korea. https://doi.org/10.1115/GT2016-56359
17. Chatterjee T, Peet Y. Effect of artificial length scales in large eddy simulation of a neutral atmospheric boundary layer flow: A simple solution to log-layer mismatch. *Phys Fluids*. 2017;29:075105. https://doi.org/10.1063/1.4994603
18. Chatterjee T, Peet Y. Contribution of large scale coherence to wind turbine power: a large eddy simulation study in periodic wind farms. *Phys Rev Fluids*. 2018;3(3). https://doi.org/10.1103/PhysRevFluids.3.034601
19. Smagorinsky J. General circulation experiments with the primitive equations. *J Mon Weather Rev*. 1963;91(3):99-164.
20. Germano M, Piomelli U, Moin P, et al. Dynamic subgrid-scale eddy viscosity model. *Phys Fluids A*. 1991;3(7):1760-1765.
21. Lilly DK. Proposed modification of the Germano subgrid-scale closure method. *Phys Fluids A*. 1991;4(3):633-635.
22. Stolz S, Schlatter P, Meyers D, Kleiser L. High-pass filtered eddy-viscosity models for LES. In: Friedrich R, Geurts B, Metais O, eds. *Direct and Large-Eddy Simulation*. Dordrecht, Netherlands: Springer; 2001:81-88.
23. Bardina J, Ferziger J, Reynolds W. Improved Turbulence Models Based on Large-Eddy Simulation of Homogeneous Incompressible Turbulent Flows [Technical Report TF-19]. Stanford, CA: Thermosciences Division, Department of Mechanical Engineering, Stanford University; 1983.
24. Sarghini F, Piomelli U, Balaras E. Scale-similar models of large eddy simulations. *Phys Fluids*. 1998;11(6):1596-1607.
25. Zang Y, Street RL, Koseff JR. A dynamic mixed subgrid-scale model and its application in turbulent recirculating flows. *Phys Fluids A*. 1993;5(12):3186-3196.
26. Geurts BJ. Inverse modelling for large eddy simulation. *Phys Fluids*. 1997;9(12):3585-3589.
27. Iliescu T, Fischer PF. Backscatter in rational LES model. *Comput Fluids*. 2006;33(5-6):783-790.
28. Stolz S, Adams NA, Kleiser L. An approximate deconvolution procedure for large-eddy simulations with application to incompressible wall-bounded flows. *Phys Fluids*. 2001;13(4):997-1015.
29. Medic G, Templeton JA, Kalitzin G. Wall modeling for LES: what turbulence information is retained. *Comput Fluids*. 2006;33(7):809-815.

30. Leray J. Essai sur mouvement dún fluide visqueux emplissant léspace. *Acta Math*. 1934;63:193-248.
31. Geurts B, Kuczaj AK, Titi ES. Regularization modelling for large-eddy simulation of homogeneous isotropic decaying turbulence. *J Phys A Math Theor*. 2008;41(34).
32. Berselli LC, Iliescu T, Layton WJ. *Mathematics of Large Eddy Simulation of Turbulent Flows*. Berlin, Germany: Springer-Verlag; 2006.
33. Guermond JL, Prudhomme S. Mathematical analysis of a spectral hyperviscosity LES model for the simulation of turbulent flows. *Math Model Numer Anal*. 2003;37(6):893-908.
34. Meneaveau C, Katz J. Scale-invariance turbulence models for large eddy simulation of boundary layers. *Ann Rev Fluid Mech*. 2000;32:1-32.
35. Boris JP, Goldstein FF, Oran ES, Kolbe RL. New insights into large eddy simulation. *Fluid Dyn Res*. 1992;10(4-6):199-228.
36. Fureby C, Grinstein FF. Monotonically integrated large eddy simulation of free shear flows. *AIAA J*. 1999;37(5):544-556.
37. Vreman AW, Geurts BJ, Kuerten JGM. Large-eddy simulation of turbulent mixing layer. *J Fluid Mech*. 1997;339:357-390.
38. Karamanos GS, Karniadakis GE. A spectral vanishing viscosity method for large-eddy simulations. *J Comput Phys*. 2000;163(1):22-50.
39. Trias FX, Gorobets A, Péres-Segara CD, Oliva A. Numerical simulation of turbulence at lower costs: regularization modeling. *Comput Fluids*. 2013;80(1):251-259.
40. Geurts BJ. Regularization modeling for LES of separated boundary layer flow. *J Fluids Structures*. 2008;24(8):1176-1184.
41. Tadmor E. Convergence of spectral methods for nonlinear conservation laws. *SIAM J Numer Anal* 1989;26(1):30-44.
42. Lions JL. *Quelques Méthodes de Résolution des Problémes aux Limites non Linéaires*. Paris, France: Dunod; 1969.
43. Ladyženskaja OA. On modification of Navier-Stokes for large velocity gradients. *Zap Nauchn Sem POMI*. 1968;7:126-154.
44. Foias C, Holm D, Titi E. The Navier-Stokes-alpha model of fluid turbulence. *Physica D*. 2001;152-153:505-519.
45. Geurts BJ, Holm DD. Leray and LANS-alpha modelling for turbulent mixing. *J Turbul*. 2006;7:10-44.
46. Visbal MR, Rizetta DP. Large-eddy simulation on curvilinear grids using compact differencing and filtering scheme. *ASME J Fluid Engg*. 2002;124(4):836-847.
47. Bogey C, Bailey C. A family of low dispersive and low dissipative explicit schemes for flow and noise computations. *J Comput Phys*. 2004;194(1):194-214.
48. Mathew J, Foysi H, Friedrich R. New approach to LES based on explicit filtering. *Int J Heat Fluid Flow*. 2006;27(4):594-602.
49. Layton WJ, Rebholz LG. Introduction. *Approximate Deconvolution Models of Turbulence: Analysis, Phenomenology and Numerical Analysis*. Berlin, Germany: Springer; 2012:1-33.
50. Fischer PF, Mullen JS. Filter-based stabilization of spectral element methods. *Comptes Rendus Acad Sci Ser I Math*. 2001;332(3):265-270.
51. Boyd JP. Two comments on filtering (artificial viscosity) for Chebyshev and Legendre spectral and spectral element methods: preserving boundary conditions and interpretation of the filter as diffusion. *J Comput Phys*. 1998;143(1):283-288.
52. Levin JG, Iskandarani M, Haidvogel DB. Spectral filtering procedure for eddy-resolving simulations with spectral element ocean model. *J Comput Phys*. 1997;137(1):130-154.
53. Deville MO, Fischer PF, Mund EH. *High-Order Methods for Incompressible Fluid Flow*. Cambridge, UK: Cambridge University Press; 2002.
54. Ladyženskaja OA. New equations for the description of motion of viscous incompressible fluids and solvability in the large of boundary value problems for them. *Boundary Value Problems of Mathematical Physics*. Providence, RI: American Mathematical Society; 1967.
55. Fischer P, Lottes J, Pointer D, Siegel A. Petascale algorithms for reactor hydrodynamics. *J Phys Conf Ser*. 2008;25(1).
56. Peet Y, Fischer P. Conjugate heat transfer LES simulations in application to wire-wrapped fuel pins. Paper presented at: 40th AIAA Fluid Dynamics Conference and Exhibit2010; Chicago, IL.
57. Peet Y, Fischer P, Conzelmann G, Kotamarthi V. Actuator line aerodynamics model with spectral elements. Paper presented at: AIAA Paper 51St Aerospace Sciences Meeting; 2013; Grapevine, TX:.
58. Obabko AV, Fischer PF, Tautges TJ, et al. Large eddy simulation of thermo-hydraulic mixing in a T-junction. In: Guillen DP, ed. *Nuclear Reactor Thermal Hydraulics and Other Applications*. Rijeka, Croatia: InTech; 2013.
59. Schlatter PC. Large eddy simulation of transition and turbulence in wall-bounded shear flow [PhD thesis]. Zürich, Switzerland: ETH Zürich; 2005.
60. Patera AT. A spectral element methods for fluid dynamics: laminar flow in a channel expansion. *J Comput Phys*. 1984;54(3):468-488.
61. Maday Y, Patera AT. Spectral element methods for incompressible Navier-Stokes equations. In: AK Noor, JT Oden, eds. *State-of-the-Art Surveys on Computational Mechanics*. New York, NY: ASME; 1989:71-143. (Chapter 3).
62. Fischer P. An overlapping Schwarz method for spectral element solution of the incompressible Navier-Stokes equations. *J Comp Phys*. 1997;133(1):84-101.
63. Tomboulides A, Lee JCY, Orszag S. Numerical simulation of low Mach number reactive flows. *J Sci Comput*. 1997;12(2):139-167.
64. Lynch RE, Rice JR. Direct solution of partial difference equations by tensor product methods. *Numer Math*. 1964;6(1):185-199.
65. Fischer PF, Lottes JW, Kerkemeier SG. Nek5000: An open source CFD solver. 2008. http://nek5000.mcs.anl.gov
66. Orszag SA. Spectral methods for problems in complex geometry. *J Comput Phys*. 1980;37(1):70-92.
67. Canuto CM, Hussaini Y, Qaurteroni A, Zhang TA. *Spectral Methods in Fluid Dynamics*. New York, NY: Springer-Verlag; 1988.
68. Meneveau C, Lund T, Cabot W. A Lagrangian dynamic sub-grid scale model of turbulence. *J Fluid Mech*. 1996;319:353-385.
69. Sagaut P. *Large Eddy Simulations for Incompressible Flows*. Berlin, Germany: Springer-Verlag; 2006.

70. Meyers J, Sagaut P. On the model coefficient for the standard and the variational multi-scale Smagorinsky model. *J Fluid Mech*. 2006;569:287-319.
71. Duchon J, Robert R. Inertial energy dissipation for weak solutions of incompressible Euler and Navier-Stokes equation. *Nonlinearity*. 2000;13(1):249-255.
72. Geurts BJ, Holm DD. Regularization modelling for large eddy simulation. *Phys Fluids*. 2003;15(1):13-16.
73. Hoyas S, Jiménez J. Scaling of velocity fluctuations in turbulent channels up to $Re_\tau = 2003$. *Phys Fluids*. 2006;18(1). https://doi.org/10.1063/1.2162185
74. Lee M, Moser RD. Direct numerical simulation of turbulent channel flow up to $Re_\tau = 5200$. *J Fluid Mech*. 2015;774:395-415.
75. Flack KA, Schultz MP, Shapiro TA. Experimental support for Townsend's, Reynolds number similarity hypothesis on rough walls. *Phys Fluids*. 2005;19(3). https://doi.org/10.1063/1.1843135
76. Jiménez J. Turbulent flow over rough walls. *Annu Rev Fluid Mech*. 2004;36:173-196.
77. Perry AE, Henbest S, Chong MS. Theoretical experimental studies of wall turbulence. *J Fluid Mech*. 1986;165:163-199.
78. Nickels TB, Marusic I, Hafez S, Chong MS. Evidence of the k^{-1} law in a high-Reynolds-number turbulent boundary layer. *Phys Rev Lett*. 2005;95(7).
79. Hutchins N, Nickels TB, Marusic I, et al. Hot-wire spatial resolution issues in wall-bounded turbulence. *J Fluid Mech*. 2009;635:103-136.
80. Stevens RJAM, Wilczek M, Meneveau C. Large eddy simulation of study of the logarithmic law for second higher order moments in turbulent wall bounded flow. *J Fluid Mech*. 2014;757:888-907.
81. Jiménez J. Cascades in wall-bounded turbulence. *Annu Rev Fluid Mech*. 2012;44:27-45.
82. Driest Van ER. On turbulent flow near wall. *J Aerospace Sci*. 1956;23(11):1007-1011.
83. Hess B, Gong J, Páll S, Peplinski A. Highly Tuned Small Matrix Multiplications Applied to Spectral Element Code Nek5000, Paper presented at: 3rd International Workshop on Sustainable Ultrascale Computing Systems; 2016; Sofia, Bulgaria.

How to cite this article: Chatterjee T, Peet YT. Regularization modelling for large-eddy simulation in wall-bounded turbulence: An explicit filtering-based approach. *Int J Numer Meth Fluids*. 2018;1–17. https://doi.org/10.1002/fld.4508

APPENDIX

COMPUTATIONAL COMPLEXITY OF LES MODELS

In this section, we document the computational complexity of the LES models (DS and FR) at each timestep added to the already existing computational cost of solving the Navier-Stokes equations. We also compare the total computational cost of the different LES solvers used.

In the following analysis, $N_x^e,\ N_y^e,\ N_z^e$ are the number of spectral elements in the x, y, z direction in a rectangular Cartesian grid, and m is the order of the polynomials (resulting in $(m+1)^3$ GLL points per element). Table A1 illustrates the computational cost per timestep of the different functions used in the 2 LES models. The cost of addition, multiplication, assignment and copy operations per timestep is of the order $\sim O(N_e(m+1)^3)$ floating point operations. The matrix multiplication used for tensor product calculations[83] in filtering for both LES models and gradient operations (calculating $\widetilde{S}_{ij}$ from velocity) in the DS model, are relatively expensive and have a computational complexity of $\sim N_e\,[3\times(2m+1)]\,(m+1)^3$. Within each element, the dense matrix multiplication can be written as

$$\mathbf{C}_{n_1\times n_3} = \mathbf{A}_{n_1\times n_2}\times\mathbf{B}_{n_2\times n_3}. \tag{A1}$$

The 3D tensor product operation[64] is a conglomerate of 3 such consecutive matrix multiplications, with $n_1 = (m+1)$, $n_2 = (m+1), n_3 = (m+1)^2$ for x direction; $n_1 = (m+1), n_2 = (m+1), n_3 = (m+1)$ for y direction, multiplied by $n_c = (m+1)$ because of matrix concatenation; and $n_1 = (m+1)^2, n_2 = (m+1), n_3 = (m+1)$ for z direction. The cost of matrix multiplication is thus $O(n_1n_2n_3)$ in the x, z direction, whereas it is $O(n_1n_2n_3n_c)$ in the y direction. Subsequently, the respective complexities in each element can be calculated as $(2m+1)(m+1)^3$ in x, y, z direction. Note that the $2m+1$ is a manifestation of $(m+1)$ multiplication followed by m addition in the innermost loop of matrix multiplication. Subsequently, 1 filtering operation or one gradient operation of one variable over the whole domain has a computational complexity of $\sim N_e\,[3\times(2m+1)]\,(m+1)^3$. The ratio of the complexity of DS to the filter-based model

TABLE A1 C_{DS}, C_{FR} are the computational complexities per timestep of the dynamic Smagorinsky and filter-based regularization models normalized by $N_e(m+1)^3$ and added to the cost of solving the Navier-Stokes equations. N_e is the number of spectral elements, and m is the order of Legendre polynomials per element. See the definition of Δ, $|\widetilde{S}|$ L_{ij}, M_{ij}, in Section 3. (i) is the 3D tensor product operations, and (ii) is the standard operations: addition, multiplication, assignment, copy

Computation	C_{DS}	C_{FR}
L_{ij}	(i) $9 \times (6m+3)$	–
	(ii)18	–
$\widetilde{S}_{ij} = 1/2\left(\frac{\partial u_i}{\partial x_j} + \frac{\partial u_j}{\partial x_i}\right)$	$3 \times (6m+3) + 81$	–
$\lvert\widetilde{S}\rvert$	19	–
M_{ij}	(i) $13 \times (6m+3)$	–
	(ii) 49	–
$C_s^2 = \frac{1}{2}\frac{\langle L_{ij}M_{ij}\rangle}{\langle M_{ij}M_{ij}\rangle}$	31	–
$\nu_t = (C_s\Delta)^2\lvert\widetilde{S}\rvert$	$i)\,4$	–
Filtering $\boldsymbol{u}, p$	–	(i) $4 \times (6m+3)$
	–	(ii) 12
Total	$150m + 277$	$24\,(m+1)$

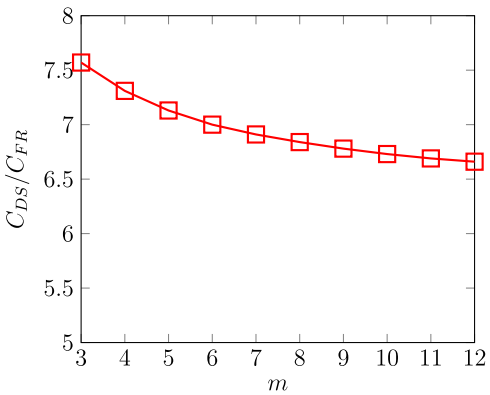

FIGURE A1 The ratio of the added computational complexity $C_{\mathrm{DS}}/C_{\mathrm{FR}}$ (dynamic Smagorinsky and filter-based regularization) for different Legendre polynomial orders m [Colour figure can be viewed at wileyonlinelibrary.com]

TABLE A2 Total computational cost of DS and FR large-eddy simulation solvers in the spectral element code Nek5000. Total time corresponds to the solver computational time to simulate $1.9T_e$ ($T_e = 8\pi\delta/U_m$ is the flow-through time), which requires 1000 steps for FR and 2000 steps for DS. $\Delta t_{\mathrm{DS}} = 1/2\Delta_{\mathrm{FR}}$. All calculations done on 256 processors, using $70 \times 20 \times 30$ spectral element grid

Case	m=5, Time/Timestep	m=5, Total Time	m=7, Time/Timestep	m=7, Total Time
DS	6.3111E-01 s	1.26222E+03 s	1.48513E+00 s	2.97026E+03
FR	6.1333E-01 s	6.1333E+02 s	1.45359E+00 s	1.45359E+03
Ratio, DS/FR	1.03	2.06	1.02	2.04

Abbreviations: DS, dynamic Smagorinsky; FR, filter-based regularization.

can be given as $\frac{C_{\mathrm{DS}}}{C_{\mathrm{FR}}} = \frac{150\,m+277}{24(m+1)}$, which is independent of the number of spectral elements and depends only on the order of polynomials. Figure A1 illustrates that $\frac{C_{\mathrm{DS}}}{C_{\mathrm{FR}}}$ decays very slowly from $\sim$ 7.57 to $\sim$ 6.66 as the order of the polynomial increases from 3 to 12. In Nek5000, a standard choice of the order of the polynomials is in the range of $m \sim 6-9$ for performing DNS and LES simulations.[13] In this range, the ratio of the added computational complexities for the 2 models is roughly $\frac{C_{\mathrm{DS}}}{C_{\mathrm{FR}}} \sim 7$.

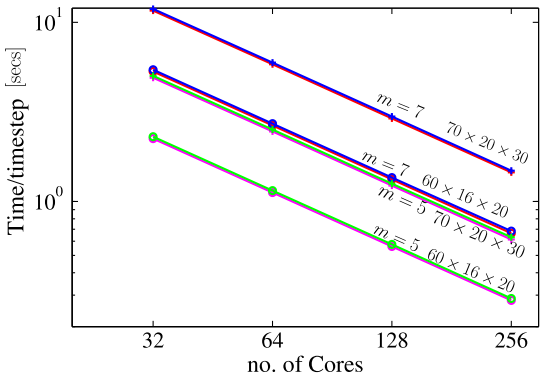

FIGURE A2 Time per timestep for dynamic Smagorinsky (blue, green) and filter-based model; $\alpha = 0.01$, $k_f = 1$ (red, magenta) for different number of cores; 32, 64, 128, 256, for 2 different grid sizes $60 \times 16 \times 20$ ($\circ$), $70 \times 20 \times 30$ ($+$); and 2 polynomial orders, $m = 5$ and $m = 7$ [Colour figure can be viewed at wileyonlinelibrary.com]

To complement the above analysis, we document the total computational cost of the 2 LES solvers in Table A2 and Figure A2, taking into account the added number of operations because of the LES modeling and the reduction of time step in the DS model due to stability restrictions. Table A2 shows that while the time per timestep is increased slightly in the DS model compared to the FR model because of a higher computational complexity of the DS model as demonstrated in Figure A1, the total computational cost of the DS solver is more than doubled compared to that of the filter-based solver because of a reduction in timestep by 2 because of stability restrictions. This analysis was conducted by running both models for a total of 1.9 flow through times. Figure A2 demonstrates the strong parallel scalability of both models, showing, again, a consistent $2 - 3\%$ increase in a computational time per timestep of the DS model as compared with the FR model on different number of processors.